

THE FAR-UV INTERSTELLAR RADIATION FIELD IN GALACTIC DISKS: NUMERICAL AND ANALYTIC MODELS

SHMUEL BIALY*

Harvard Smithsonian Center for Astrophysics, 60 Garden st., Cambridge, MA, 02138

ApJ. Accepted (Sept 10, 2020)

ABSTRACT

The intensity of the far-ultraviolet (FUV; 6-13.6 eV) interstellar radiation field (ISRF) in galaxies determines the thermal and chemical evolution of the neutral interstellar gas and is key for interpreting extragalactic observations and for theories of star-formation. We run a series of galactic disk models and derive the FUV ISRF intensity as a function of the dust-to-gas ratio, star-formation rate density, gas density, scale radius, and observer position. We develop an analytic formula for the median FUV ISRF flux. We identify two dimensionless parameters in the problem: (1) the dimensionless galactic radius, X , which measures the radial extent of FUV sources (OB stellar associations) in the disk; (2) the opacity over the inter-source distance, τ_* , which measures the importance of dust absorption. These parameters encapsulate the dependence on all of the physical parameters. We find that there exists a critical τ_* , or equivalently a critical dust-to-gas ratio, $Z'_{d,crit} \approx 0.01 - 0.1$ the Milky Way value, at which the ISRF changes behavior. For $Z'_d > Z'_{d,crit}$ the ISRF is limited by dust absorption. With decreasing Z'_d , the ISRF intensity increases as more sources contribute to the flux. For $Z'_d < Z'_{d,crit}$ the ISRF saturates as the disk becomes optically thin. We find that the ISRF per star-formation rate density in low metallicity systems, such as dwarf and high redshift galaxies, is higher by up to a factor of 3-6 compared to their Milky-Way counterparts. We discuss implications to the potential mechanisms that regulate star-formation in low metallicity galaxies.

Subject headings: galaxies: ISM – galaxies: star formation – ISM: general – dust, extinction – methods: analytical – methods: numerical

1. INTRODUCTION

Massive stars are responsible for the generation of the far-ultraviolet (FUV; 6 – 13.6 eV) interstellar radiation field (ISRF) in galaxies. The intensity of the FUV ISRF is a key property of the interstellar medium (ISM) of galaxies. It shapes the thermal and chemical structure of the ISM and may be key for regulating the star-formation rate (SFR). The FUV radiation is typically the dominant heating source of the neutral ISM, through the photoelectric ejection of electron off dust grains (Bakes & Tielens 1994), and it thus controls the thermal state of interstellar gas and the balance between the warm-cold neutral media (WNM/CNM) phases (Wolfire et al. 1995; Liszt 2002; Wolfire et al. 2003; Hill et al. 2018; Bialy & Sternberg 2019). The FUV photoelectric heating introduces a natural feedback loop for star formation in galactic disks, where any increase in the star-formation rate (SFR) results in an increased gas heating rate which reduces the abundance of the cold (and dense) phase reducing back the SFR (Corbelli & Salpeter 1988; Parravano 1988, 1989; Ostriker et al. 2010).

Subsequent studies (Kim et al. 2011; Ostriker & Shetty 2011; Shetty & Ostriker 2012; Kim et al. 2013; Kim & Ostriker 2015, 2017), stressed the importance of supernova (SN) feedback as a regulation mechanism for star-formation. These studies find that momentum injection by SNe generates turbulent pressure that exceeds the thermal pressure, suggesting that SN feedback, rather than FUV photoelectric heating, is the dominant driver of star-formation. Interestingly, we find that in low metallicity systems (such as dwarfs and high redshift galaxies) the ratio of the FUV ISRF per SFR is elevated by a factor of 3-6 (compared to Milky-Way-like galaxies), implying that the thermal pressure in these systems may be

come important and that the FUV photoelectric heating may be the dominant self-regulation process of star-formation (see §4.2 for an elaborate discussion). A key factor in the self-regulation theory is the ratio of the FUV ISRF intensity to the SFR density. While often assumed to be constant, we show that this ratio varies with galaxy properties: the gas density, SFR, dust-to-gas ratio (DGR), and galactic scale radius. In this paper we characterize this dependence through a set of numerical calculations, and an analytic model.

The intensity of the FUV ISRF also determines the chemical evolution of atomic and molecular clouds in the ISM, and the intensity of molecular radio and sub-millimeter emission lines through photo-excitation and photo-dissociation of various molecular energy levels at the edges of photodissociation regions (PDRs Tielens & Hollenbach 1985; Hollenbach & Tielens 1999). A model of the FUV ISRF is thus required for an accurate interpretation of extragalactic observations tracing the atomic/molecular ISM. In particular, the FUV intensity is a key parameter for the process of atomic-to-molecular (HI-to-H₂) transition (Glassgold & Langer 1974; Draine & Bertoldi 1996; Krumholz et al. 2008; McKee & Krumholz 2010; Sternberg et al. 2014; Bialy & Sternberg 2016; Bialy et al. 2017), which may regulate and/or trace star-formation (e.g., Leroy et al. 2008; Bigiel et al. 2008; Gnedin et al. 2009; Glover & Clark 2012; Kuhlen et al. 2012; Diemer et al. 2019).

The FUV ISRF is the summed contribution of FUV fluxes from OB stellar associations, down-weighted by the effect of dust absorption (Parravano et al. 2003, hereafter PHM). As such, the FUV ISRF is a function of various physical parameters that characterize the galaxy: the dust-to-gas ratio (DGR) or the galaxy metallicity, the gas mean density, and the density of OB stellar associations which is in turn related to the SFR. The aim of this paper is to develop an analytic model to de-

*sbialy@cfa.harvard.edu

scribe the FUV ISRF intensity as a function of these physical properties.

The structure of the paper is as follows. We describe the model ingredients and our numerical calculations in §2. In this section we also identify the governing dimensionless parameters and connect them to the physical parameters, the SFR density, the gas density, the DGR and the OB stars scale radius. In §3 we present the numerical results and derive an analytic formula for the FUV ISRF. We do so in increasing steps of complexity, starting from an idealized model of an observer located in the disk center, and FUV sources of constant luminosity (§3.1). We then generalize the theory to: 1) account for a source luminosity distribution that resembles that of realistic OB stellar associations (§3.2), and 2) to describe off-central observers (e.g., the sun in the Milky-Way galaxy) where the polar symmetry of the problem is broken (§3.4). We summarize our model and discuss implications to star-formation self-regulation and potential model extensions in §4. We conclude in §5.

2. MODEL INGREDIENTS

Here we discuss the basic model ingredients for the derivation of the FUV ISRF for galaxies of different properties: galaxy radius, DGR, and SFR. We assume a thin exponential disk, in which we randomly distribute radiation sources (see §2.3 for more details), where the radiation sources represent associations of OB stars. At a given point in the disk, \vec{r} , the FUV ISRF is the sum of all FUV radiation sources, and is given by

$$F(\vec{r}) = \sum_i \frac{L_i e^{-\sigma n |\vec{r}_i - \vec{r}|}}{4\pi |\vec{r}_i - \vec{r}|^2}, \quad (1)$$

where \vec{r}_i and L_i are the position and luminosity of each source. In the exponent, σ is the dust absorption cross-section per hydrogen nucleus (over the FUV band), and n is the mean hydrogen nucleus density of the gas. Assuming an exponential disk, the surface density of FUV sources decreases as

$$N_*(r) = N_{*,c} e^{-r/R_{\text{gal}}}, \quad (2)$$

where $N_{*,c}$ is the central surface density, and R_{gal} is the exponential scale-radius of OB associations.

Since OB associations vary in mass and luminosity, there is no single value for the source luminosity, L_i . We adopt the probability density function (PDF)

$$\frac{dp}{dL} = \frac{1}{\Lambda - 1} \frac{L_{\text{max}}}{L^2} \quad (3)$$

when $L_{\text{min}} \leq L \leq L_{\text{max}}$, and $dp/dL = 0$ otherwise. Here L_{min} , L_{max} are the luminosities of the least and most luminous associations, and

$$\Lambda \equiv L_{\text{max}}/L_{\text{min}} = 5900. \quad (4)$$

This source luminosity distribution is derived from the distribution of number of stars in OB associations discussed in PHM¹, based on the McKee & Williams (1997) model. The mean luminosity per source is $\langle L \rangle = \ln \Lambda / (\Lambda - 1) L_{\text{max}} = 8.7 L_{\text{min}} = 1.5 \times 10^{-3} L_{\text{max}}$.

¹ We obtain the cumulative distribution for luminosity larger than L by following Eq. 15 in PHM, and expressing the distribution in terms of association luminosity assuming it is proportional to the number of massive stars in it.

2.1. Governing Dimensionless parameters

In this subsection we identify the dimensional and dimensionless quantities. We use them to rewrite the problem in dimensionless form (Eq. 16 below). This makes our results more general and allow for future variations and extensions to our model (see §4.3 for a discussion).

The natural flux unit is the source emissivity

$$\Sigma_* \equiv \langle L \rangle N_* \quad (5)$$

where N is the surface density of all FUV sources (i.e., OB associations of any luminosity) at the position of the observer. There are three distance scales that naturally appear in the problem: (a) the inter-source scale

$$l_* \equiv N_*^{-1/2}, \quad (6)$$

(b) the dust-absorption length-scale

$$R_d \equiv 1/(\sigma n), \quad (7)$$

and (c) the galactic scale radius, R_{gal} . These length-scales may be combined to give two independent dimensionless parameters, which characterize the problem:

$$\tau_* \equiv l_*/R_d = \sigma n l_* \quad (8)$$

$$\tau_{\text{gal}} \equiv R_{\text{gal}}/R_d = \sigma n R_{\text{gal}}$$

These parameters are the dust opacity over the inter-source distance, and the dust opacity over the galactic scale radius, respectively. Alternatively, we will often use the combination of the parameters: τ_* and the dimensionless galactic radius,

$$X \equiv R_{\text{gal}}/l_* = \tau_{\text{gal}}/\tau_* \quad (9)$$

X measures the extent of OB stellar associations in the galactic disk, and is independent of the dust abundance.

2.2. Connection to Physical Units

The values of τ_* and X (and τ_{gal}) depend on the DGR, gas density, and the SFR density. These parameters may vary for galaxies of different masses, evolutionary stages, and with cosmic epoch, as well as with galactocentric radius, for a given galaxy.

Assuming that the surface density of OB associations is proportional to the SFR surface density we write

$$N_* = 6.8 \times 10^{-5} \Sigma'_{\text{sfr}} \text{ pc}^{-2}, \quad (10)$$

where Σ'_{sfr} is the SFR surface density normalized to solar circle, and the normalization $N_{*,\odot} = 6.8 \times 10^{-5} \text{ pc}^{-2}$ is the total density of OB associations at the solar circle (PHM). We adopt a mean source luminosity $\langle L \rangle = 1.8 \times 10^5 L_{\odot}$, giving a source emissivity

$$\Sigma_* = N_* \langle L \rangle = 12 \Sigma'_{\text{sfr}} L_{\odot} \text{ pc}^{-2}, \quad (11)$$

in good agreement with PHM who obtain $\Sigma_* = 10.9 L_{\odot} \text{ pc}^{-2}$ for the solar circle. With these assumed values for $N_{*,\odot}$ and $\langle L \rangle$, our numerical calculations recover the observed FUV ISRF, $F_{\odot} = 2.7 \times 10^{-3} \text{ erg cm}^{-2} \text{ s}^{-1}$ (Draine 1978), for solar neighborhood conditions.

For a given SFR density, gas density, and DGR,

$$l_* = N_*^{-1/2} = 121 \Sigma'_{\text{sfr}}^{-1/2} \text{ pc} \quad (12)$$

$$R_d = 1/(\sigma n) = 324 (n_0 Z'_d)^{-1} \text{ pc},$$

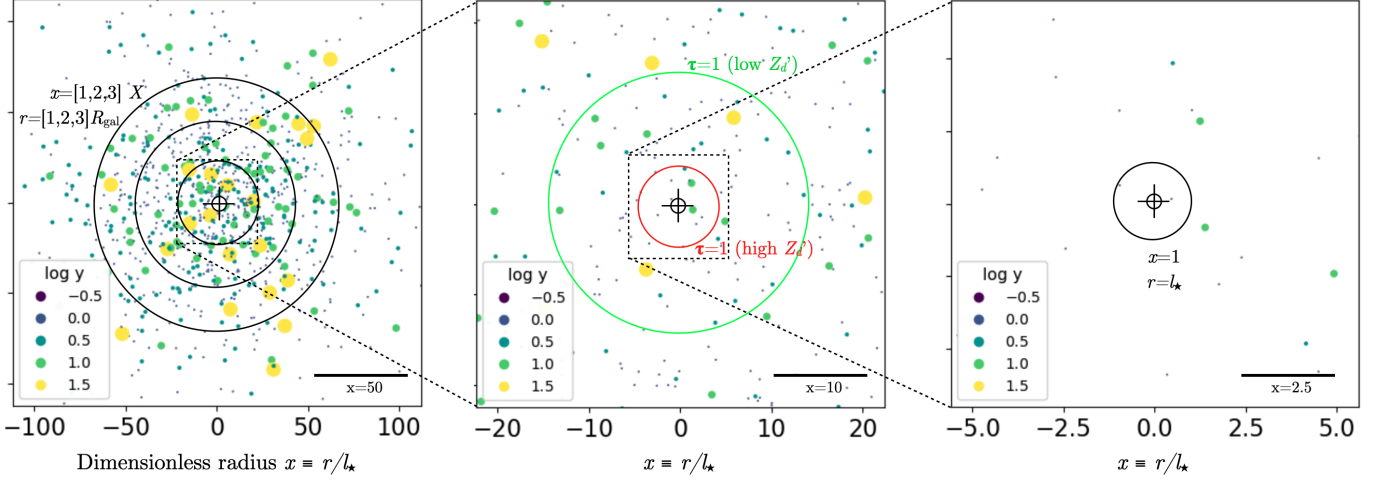


FIG. 1.— One random realization (out of 20k for each model) of OB associations in an exponential disk as given by our numerical model. The $x-y$ coordinates are in units of the inter-source distance l_* (see Eq. 16). The colored markers (also vary in size) show the associations binned by $\log_{10} y$ where $y \equiv L/\langle L \rangle$ following Eq. (17). Also shown are the galactic scale radii $r = [1, 2, 3]R_{\text{gal}}$ (i.e., $x = [1, 2, 3]X$) (left panel), the dust-absorption radius where $\tau = 1$ (i.e., $r = R_d$ or $x = \tau_*^{-1}$) (middle-panel), and the inter-source scale $r = l_*$ (or $x = 1$) (right-panel).

where we defined $n_0 \equiv n/(\text{cm}^{-3})$, and assumed $\sigma = 10^{-21} Z'_d \text{ cm}^2$ where Z'_d is the DGR normalized to the solar circle value. The value of l_* represents a characteristic distance between OB associations (of any luminosity)². The dimensionless parameters

$$\begin{aligned} \tau_* &= \sigma n l_* = 0.37 n_0 Z'_d \Sigma_{\text{sfr}}'^{-1/2} \\ \tau_{\text{gal}} &= \sigma n R_{\text{gal}} = 3.1 n_0 Z'_d R_{\text{gal,kpc}} \\ X &= R_{\text{gal}}/l_* = 8.2 R_{\text{gal,kpc}} \Sigma_{\text{sfr}}'^{1/2} \end{aligned} \quad (13)$$

where $R_{\text{gal,kpc}} \equiv R_{\text{gal}}/\text{kpc}$. For solar neighbourhood conditions $n_0 \approx 1$, $\Sigma_{\text{sfr}}' = Z'_d = 1$ (by definition), and we get $l_{*\odot} \approx 121$ pc, and $\tau_{*\odot} \approx 0.37$. Assuming an OB galactic scale radius $R_{\text{gal}} = 3.5$ kpc (Wolfire et al. 2003), we further obtain $X_{\odot} \approx 29$ for the solar-circle. The values of the parameters above depend on the SFR density, gas density, DGR and galactic scale radius. With increasing gas density and/or DGR, the effective dust-absorption scale, R_d , decreases and the opacities, τ_* and τ_{gal} , rise. As Σ_{sfr}' increases the density of sources increases, leading to a lower l_* and τ_* , and a higher X . Finally X also increases with the galactic scale radius of OB associations.

While τ_* and X are expected to vary for different galaxies, they also vary within a galaxy, with varying galactocentric radius of the observer, R_{obs} . In Eq. (13) this dependence is encapsulated in the SFR density parameter, where $\Sigma_{\text{sfr}}' \propto N_* \propto e^{-R_{\text{obs}}/R_{\text{gal}}}$. Defining the dimensionless observer radius

$$\delta \equiv R_{\text{obs}}/R_{\text{gal}} \quad (14)$$

the values of l_* , τ_* and X at the observer position are related to the disk center values through

$$\begin{aligned} l_*/l_{*c} &= \tau_*/\tau_{*c} = e^{+0.5\delta} \\ X/X_c &= e^{-0.5\delta}, \end{aligned} \quad (15)$$

² Since the probability per association strongly decreases with L , N_* is dominated by under-luminous associations (compared to $\langle L \rangle$), and l_* is also a typical distance for these associations. Super-luminous associations are more rare and have a larger l_* value.

where l_{*c} , τ_{*c} , and X_c are the parameter values at disk center³. These scalings are necessarily idealized. Realistic galaxies may have regions that do not follow Eq. (2) (e.g., the central region in the Milky-Way), as well as include additional dependence on δ due to variations in the DGR and gas density. Nevertheless, we shall adopt this exponential model as it allows the derivation of generic scaling relations across a large range of physical conditions.

2.3. Numerical Method

We calculate the FUV ISRF numerically for a large set of galaxy disk models, considering different realization of the radiation sources and placing the observer in various locations within the disk. To this end we solve the dimensionless form of Eq. (1). Defining the dimensionless: flux $f = F/\Sigma_{*c}$, distance $x \equiv r/l_{*c}$, and source luminosity $y \equiv L/\langle L \rangle$, Eq. (1) takes the form

$$f(\vec{x}) = \sum_i \frac{y_i e^{-\tau_{*c} |\vec{x} - \vec{x}_i|}}{4\pi |\vec{x} - \vec{x}_i|^2}. \quad (16)$$

where the subscripts c refer to the parameters at disk center. The dimensionless source luminosity follow the PDF

$$\frac{dp}{dy} = \frac{1}{\ln \Lambda} \frac{1}{y^2}, \quad (17)$$

for $y_{\text{min}} \leq y \leq y_{\text{max}}$ and 0 otherwise, where $y_{\text{min}} = (\Lambda - 1)/(\Lambda \ln \Lambda)$ and $y_{\text{max}} = (\Lambda - 1)/(\ln \Lambda)$. By definition, $\langle y \rangle = 1$. In these dimensionless units, the distance between sources (at the disk center) is of order unity, the galactic scale radius is X_c , and the total number of sources is $2\pi X_c^2$. Thus, each galaxy disk model is characterized by two dimensionless numbers: τ_{*c} and X_c . While τ_{*c} and X_c totally define each of the galaxy disk models, f also depends on the observer position δ .

We consider 13×7 models, corresponding to all (τ_{*c}, X_c) pairs within the arrays $\log_{10}(\tau_{*c}/\tau_{*c,0}) = [-2.5, -2.25, \dots, 0.5]$ and $\log_{10}(X_c/X_{c,0}) = [-1, -0.75, \dots, 0.5]$ where $\tau_{*c,0} = 0.11$, $X_{c,0} = 96$ is our fiducial model for which the solar-circle conditions are recovered at $R_{\text{obs}} = 8.5$ kpc

³ Throughout the paper when we include a subscript c it means the parameters are evaluated at disk center. Otherwise, they are evaluated at the observer position.

(see §2.2). These 91 models represent galaxies of various DGR, gas density, SFRs and galactic radii. For each model we follow the steps:

1. We randomly distribute sources within a two-dimensional disk with an exponentially decreasing source density (Eq. 2). The source luminosities are randomly drawn from the luminosity PDF (Eq. (17)).
2. We calculate f numerically following Eq. (16), considering 7 different observer positions: $\delta = 0, 0.5, 1, 1.5, 2, 2.4, 3$ ($\delta = 2.4$ corresponds to the solar circle).
3. We repeat steps (1-2), 20,000 times to obtain many realizations of source luminosity and positions in the disk. These realizations capture fluctuations in the source distribution as new OB associations continuously form while old ones decay. From the 20k realizations we obtain the distribution of f and calculate the median and interquartile range (IQR) for each galaxy model.
4. We translate f to physical units via $F = \Sigma_{*c} f$ (Eq. 11). We derive the normalized ISRF-to-SFR ratio $I_{UV}/\Sigma'_{\text{sfr}}$ where $I_{UV} \equiv F/F_{\odot}$ is the ISRF in units of the solar neighbourhood value.

In Fig. 1 we show an example of a single random realization of FUV sources in an exponential disk model with $X = 21$, with various levels of zoom-in. The relative source luminosities, $y \equiv L/\langle L \rangle$, are drawn from the y -PDF (Eq. 17), as indicated by the marker-color and marker-size binning (see legend). In the left-panel (large-scale view) we mark the exponential decline of the source density by showing three circles that correspond to $x = [1, 2, 3]X$ (or equivalently, $r = [1, 2, 3]R_{\text{gal}}$). The value of τ_* determines the “radius of influence” within which radiation may travel freely from the sources to the observer (for $x \gg \tau_*^{-1}$ the fluxes vanish due to dust-absorption). Depending on the value of τ_* this radius may be small or large. This is shown in the middle panel. Finally, in the right-panel we show a closeup view. Here we mark the inter source distance, $x = 1$ (or $r = l_*$), which resembles the typical FUV source separation distance.

In addition to the models with the realistic source luminosity distribution, we also run models of constant source luminosity, $y_i = 1$, which we use to test our analytic model in the next section.

3. RESULTS

In this section we present our numerical results for the median FUV ISRF, and the IQR (25-75 percentile range), as functions of galactic properties as captured by the τ_* and X parameters, for various observer positions. We also derive an analytic model for the median ISRF. We start with the basic model which assumes constant luminosity sources, and a central observer (§3.1), and then we generalize the model to the case of a source luminosity distribution, and off-disk-center observers (§§3.2, 3.4).

3.1. Basic analytic Model

To obtain an analytic solution for the ISRF we need to make simplifying assumptions: We assume that the observer is located at disk center. The problem then obeys polar symmetry. We assume the sources all have the same luminosity (i.e., $y_i = 1$ in Eq. 16). Finally, we approximate Eq. (16) as the sum

of two components, the contribution of the nearest source plus an integral over the contribution of the rest of the sources. We get

$$\begin{aligned} \frac{F}{\Sigma_*} &= \frac{1}{4\pi x_0^2} e^{-x_0 \tau_*} + \int_0^{2\pi} \int_{x_0}^{\infty} \frac{1}{4\pi x} e^{-\tau_* x} e^{-x/X} dx d\theta \quad (18) \\ &= \frac{1}{4\pi x_0^2} e^{-x_0 \tau_*} + \frac{1}{2} E_1 \left(x_0 \tau_* + \frac{x_0}{X} \right), \end{aligned}$$

where E_1 is the first exponential function. The parameter x_0 is the typical (median) distance at which the nearest source is found. For randomly placed sources, the number of sources within a given area follows the Poisson distribution. The area, a_0 , within which the median number of sources is 1, is obtained from the solution to the quadratic equation $(N_* a_0)^2 - (2/3)(N_* a_0) - 0.02 = 0$, giving $N_* a_0 = 0.695$. The corresponding dimensionless radius is

$$x_0 = \sqrt{a_0 N_* / \pi} \approx 0.47. \quad (19)$$

In Eq. (18) we deliberately omitted the subscripts, c (indicating the disk center). While in our derivation we assumed a central observer, as we discuss below, Eq. (18) may be also applied to off-center observers under a simple transformation (see §3.4)

The two exponential factors in Eq. (18) account for the exponential attenuation due to dust absorption, and the decrease of the source density with galactocentric radius. The relative importance of these factors introduces two important limiting cases for Eq. (18):

1. The weak dust-absorption regime: $\tau_{\text{gal}} = \tau_* X \ll 1$
2. The strong dust-absorption regime: $\tau_{\text{gal}} = \tau_* X \gg 1$

The critical point that defines the transition for the two regimes is $\tau_{\text{gal}} = 1$, or

$$\tau_{*,\text{crit}} = 1/X. \quad (20)$$

This corresponds to the point at which the dust-scale $R_d = 1/(\sigma n)$ is comparable to the galaxy scale radius R_{gal} . This occurs at

$$Z'_{d,\text{crit}} = 0.32(n_0 R_{\text{gal,kpc}})^{-1}. \quad (21)$$

I.e., at a DGR $\approx 10\%$ the Milky-Way value (for $R_{\text{gal,kpc}} = 3.5$). We shall now discuss these two limiting cases.

3.1.1. The weak dust-absorption limit

In this limit $\tau_{\text{gal}} \ll 1$ and dust absorption is negligible over galactic scales. The ISRF depends only on X and is independent of τ_* , as the flux is limited by the galaxy scale-radius, i.e., by the exponential decline of the density of FUV sources. This limit applies to low metallicity and/or small galaxies, e.g., dwarf galaxies and some high redshift galaxies.

In this limit, the first term inside the argument of E_1 is negligible and we get $F/\Sigma_* \simeq 0.36 + 0.5E_1[0.47/X]$ (since $\tau_* \ll \tau_{\text{gal}}$, the exponent in the first term is ≈ 1). The contribution of the nearby source (first term) is typically small compared to the summed contribution of all the rest of the sources (the integral). Their ratio is $0.72/E_1(0.47/X) = 4.6$ to 8.1% , where the numerical values correspond to $X = 300$ to 30 . For large X we may also expand E_1 . To leading order $F/\Sigma_* \propto \ln(X)$. This logarithmic dependence reflects the fact that within $l_* < r < R_{\text{gal}}$, the contribution per radial ring falls

off as $1/r$, as the flux from each source is $\propto r^{-2}$ while the number of sources within $(r, r + dr)$ is $\propto r$. Indeed, if instead of an exponential disk we assume a constant density disk with a finite radius R_{gal} the integral is $\propto \int (1/r) dr = \ln(R_{\text{gal}}/l_*)$, where l_* and R_{gal} are the minimum and maximum distances to the radiation sources.

3.1.2. The Strong dust-absorption limit

In this limit $\tau_{\text{gal}} \gg 1$ and the ISRF is independent of X and depends only on τ_* , as the flux is limited by dust absorption. In other words, the characteristic distance at which dust-absorption becomes important, $R_d = 1/(\sigma n)$, is much smaller than the galactic scale radius R_{gal} . This is the limit that applies to the Milky-Way, for which $Z'_d > Z'_{d,\text{crit}}$ (Eq. 21).

In this limit $F/\Sigma_* \simeq 0.36e^{-0.47\tau_*} + 0.5E_1[0.47\tau_*]$. The relative contribution of the nearest source may become substantial, especially at large τ_* . For τ_* ranging from 0.05 to 0.5 the ratio of the first to second term ranges from 8.9 to 24 %. The E_1 function may be expanded if τ_* is small. To leading order, the integral is $\propto \ln(1/\tau_*) = \ln(R_d/l_*)$. This is similar to what one gets for a constant density disk of radius R_d . Thus, in the strong-dust absorption limit, dust absorption plays the role of an effective galactic edge.

3.2. Generalization to a Source luminosity distribution

When considering a luminosity distribution for the sources, we can no longer approximate Eq. (1) as a sum of two contributions as we did in Eq. (18). This is because the probability per unit area to encounter a source depends on its luminosity (e.g., higher luminosity associations are less likely; Eq. 17), and thus x_0 becomes a function of y . An approximate analytic expression may be derived by using an effective value

$$x_0 \rightarrow \bar{x}_0 = 0.90, \quad (22)$$

in Eq. (18). This effective value is larger than x_0 because the nearest sources are typically of very low luminosity ($y_i \ll 1$), and a larger distance is required to achieve an appreciable contribution to the flux. This is illustrated in Fig. 2, where we plot the calculated cumulative median flux as a function of the source distance, for the case of constant luminosity sources and a luminosity distribution. For constant luminosity sources, F/Σ_* experiences a significant jump at $x = x_0$ from 0 to $e^{-\tau_* x_0}/[4\pi x_0^2]$ as the first source is encountered. On the other hand, in the case of a source luminosity distribution, the first source has a typical luminosity $y \approx y_{\text{min}} \ll 1$, and thus it induces only a very mild jump in the flux (barely visible in the figure) and the flux builds up gradually with increasing x . The effective distance \bar{x}_0 reflects this smoothing effect. Comparing the numerical and analytic results we find that over most of our parameter space, the agreement is within $\lesssim 10\%$ (see Fig. 5).

Fig. 2 also shows that the cumulative fluxes saturate shortly after the distance $x = 1/\tau_*$ is reached. This corresponds to the condition that the dust optical depth $\tau = 1$. This is in agreement with the strong dust absorption limit, where dust limits the integral of the flux. Indeed the displayed model has $\tau_* = 0.11$ and $X = 96$ so that $\tau_* \gg \tau_{*,\text{crit}}$, corresponding to the strong-dust absorption regime.

3.3. The I_{UV} to star-formation rate ratio

We now rewrite the normalized flux in Eq. (18) in physical units. Defining $I_{\text{UV}} \equiv F/F_0$ where $F_0 = 2.7 \times 10^{-3} \text{ erg cm}^{-2}$

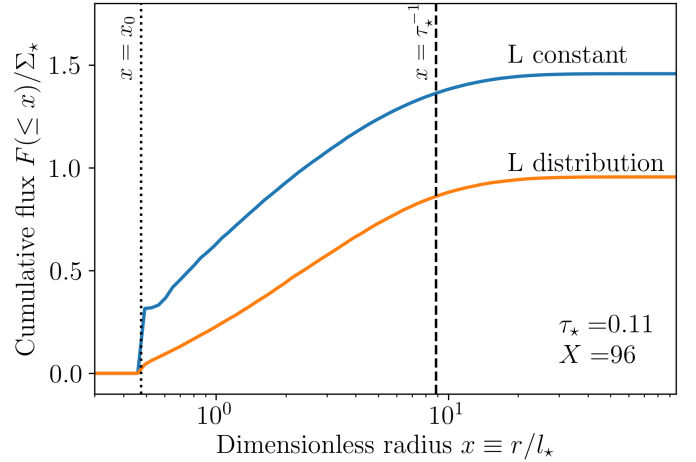


FIG. 2.— The cumulative flux (median) as a function of dimensionless distance from the source $x \equiv r/l_* = \tau/\tau_*$, for our fiducial Milky-Way model ($\tau_* = 0.11, X = 96$). The two vertical lines show the location where the nearest source is encountered ($x_0 = 0.47$), and the point where the optical depth approaches unity ($x = 1/\tau_*$), past which the ISRF saturates. The two curves correspond to a model with constant luminosity FUV sources, and to a model where the sources are described by a luminosity PDF (Eq. 17), representing the luminosity of OB stellar associations. While in the constant luminosity source model there is a jump in the ISRF at $x = x_0$ due to the contribution of the nearby source, for a source luminosity distribution the nearby FUV source typically has a low luminosity and thus the increase is gradual.

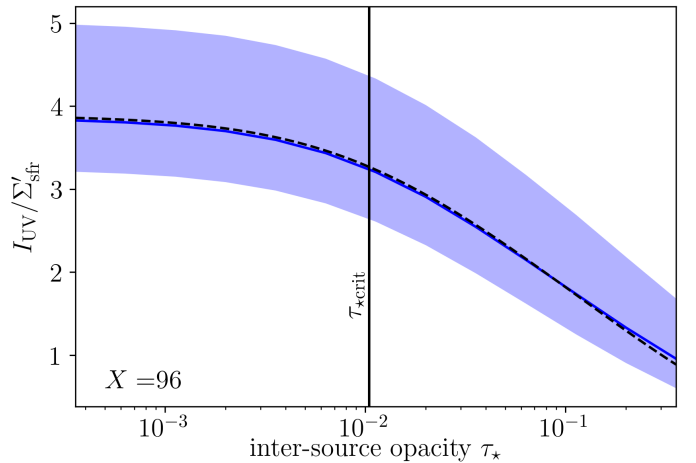


FIG. 3.— The FUV ISRF intensity to SFR density ratio (normalized to solar circle values) as a function of the inter-source dust opacity τ_* assuming $X \equiv R_{\text{gal}}/l_* = 96$ and a central observer. The solid curve and the shaded region are the median and the IQR as obtained by our numerical simulation. The dashed curve is the analytic model (Eq. 22, 23). The vertical line shows the critical $\tau_{*,\text{crit}}$ (Eq. 20) above which the ISRF limited by dust absorption. For $\tau_* \ll \tau_{*,\text{crit}}$ the ISRF saturates and becomes independent of τ_* .

s^{-1} is the solar neighborhood ISRF (Draine 1978), and with $\Sigma_* = 12 \Sigma'_{\text{sfr}} L_{\odot} \text{ pc}^{-2}$ (Eq. 11), we get

$$\frac{I_{\text{UV}}}{\Sigma'_{\text{sfr}}} = 0.91 \left(\frac{e^{-\tau_* \bar{x}_0}}{2\pi \bar{x}_0^2} + E_1 \left[\bar{x}_0 \tau_* + \frac{\bar{x}_0}{X} \right] \right). \quad (23)$$

where $\bar{x}_0 = 0.9$ and τ_* and X encapsulate the dependence on the DGR, SFR and galactic scale radius (Eq. 13). The $I_{\text{UV}} - \Sigma'_{\text{sfr}}$ ratio expresses how much FUV interstellar radiation flux is gained per massive star formed.

The $I_{\text{UV}} - \Sigma'_{\text{sfr}}$ ratio as a function of τ_* (at our fiducial $X = 96$) is shown in Fig. 3. The solid and dashed curves are the median values as obtained from our numerical sim-

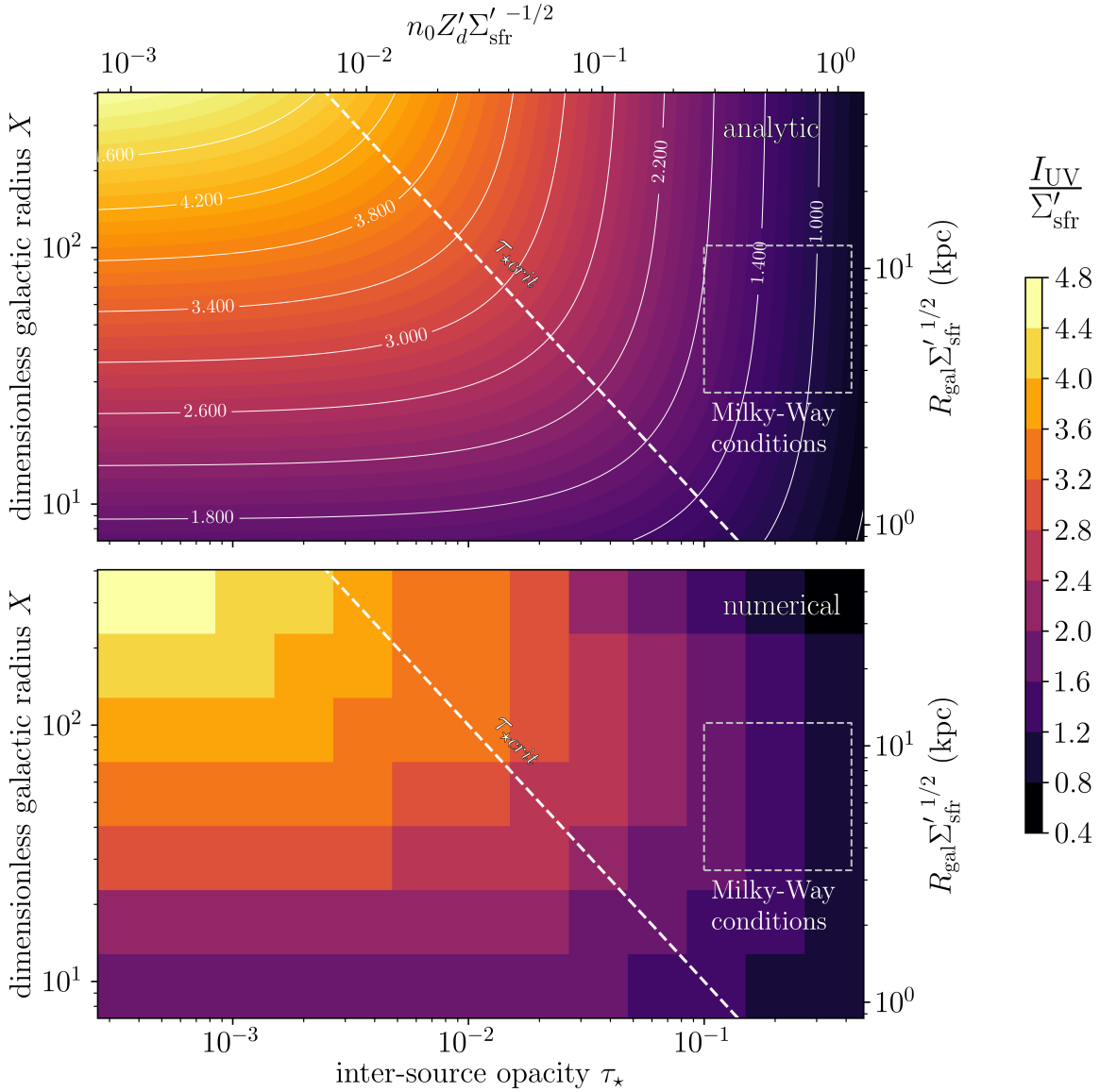


FIG. 4.— The FUV ISRF to the SFR density ratio (normalized to solar circle), I_{UV}/Σ'_{sfr} , in the τ_* – X parameter space, as given by the analytic model, Eq. (23) (top) and as obtained by our numerical simulations (bottom), assuming a central observer ($\delta = 0$). On the x -axis, τ_* is proportional to the DGR, and on the y -axis, X is proportional to the galactic scale radius, as shown by the secondary axis (and Eq. 13). The dashed rectangle marks typical conditions for the Milky-Way disk. The diagonal line is $\tau_{*,crit} = 1/X$ (Eq. 20, 21) which separates “the weak” (to the left) and “the strong” (to the right) dust absorption regimes. For $\tau_* > \tau_{*,crit}$ dust absorption controls the intensity of the ISRF. In this limit, I_{UV}/Σ'_{sfr} increases with decreasing τ_* , and is independent of X . In the opposite limit, the ISRF is controlled by the galaxy scale. I_{UV}/Σ'_{sfr} then increases with X and is independent of τ_* .

ulations, and our analytic model, Eq. (23), respectively. They are in excellent agreement. The dashed line shows $\tau_{*,crit}$ as given by Eq. (20). To the right of this line we are in the strong dust absorption limit. As expected, in this regime the median I_{UV}/Σ'_{sfr} increases as τ_* decreases, and as dust absorption becomes less efficient and allows larger regions of the galaxy disk to contribute to the ISRF. As τ_* decreases below $\tau_{*,crit}$, the galactic disk becomes optically thin and the ISRF saturates.

The shaded region in Fig. 3 is the IQR as obtained from our numerical simulations. It is a measure of the dispersion in the intensity of the FUV ISRF. These fluctuations in I_{UV} result from random fluctuations in the positions and luminosities of the FUV sources in respect to the observer, as captured by the different realizations of the FUV source distributions in our numerical models (see Fig. 1 for an example

of one such realization). These fluctuations reflect the fact that (a) for a given observer position, the distribution of FUV sources changes as OB stars form and die with time (PHM), and (b) at a given instant of time, the distance to FUV sources changes for variations in the observer position. The IQR spans $\Delta(I_{UV}/\Sigma'_{sfr}) \approx 1.1$ at high τ_* , and ≈ 1.8 at low τ_* . However, when divided by the median value, the relative dispersion decreases with decreasing τ_* , from 1.1 at high τ_* , to 0.46 at low τ_* . This is because fluctuations in the ISRF are dominated by nearby FUV sources. As τ_* decreases, far-away sources contribute more to the ISRF, and thus the relative dispersion in I_{UV} decreases.

In Fig. 4 we show the I_{UV}/Σ'_{sfr} ratio (median) in the 2-dimensional τ_* – X parameter space, as given by our analytic model (Eq. 23) (top), and by our numerical simulations (bottom). Over most of the parameter space the two agree to

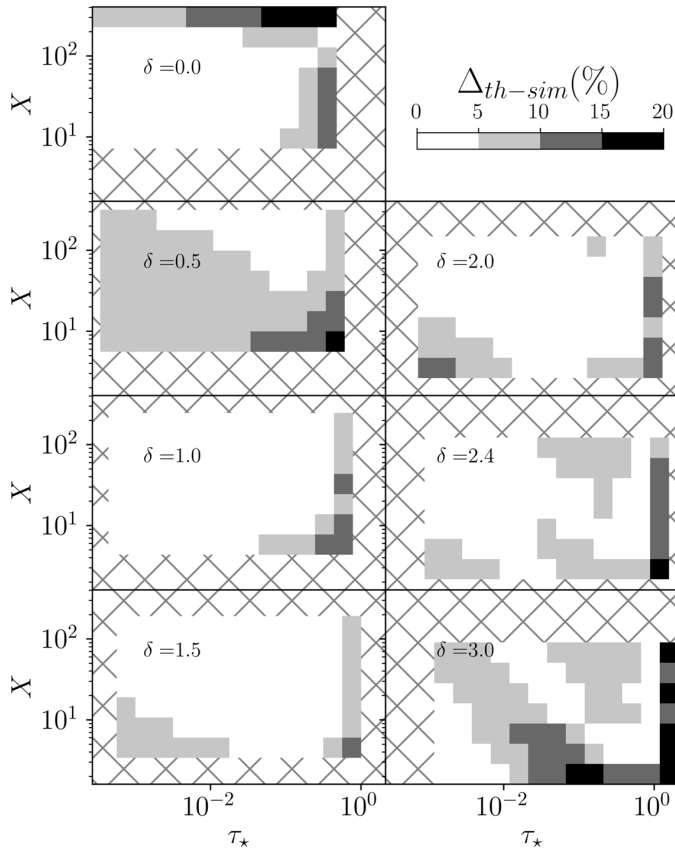


FIG. 5.— Comparison of our extended analytic model (Eq. 23, 26) with our numerical results. We show the relative difference in I_{UV}/Σ'_{sfr} ($\|\text{Theory-Simulations}\|/\text{Simulations}$) as a function of τ_* , X and observer position δ . The hatched regions are regions outside the numerical model parameter space.

within 5% (see upper-left panel of Fig. 5). The dashed rectangle shows typical conditions for the Milky-Way. The diagonal line is the critical line, $\tau_{*crit} = 1/X$ that separates the parameter space into the weak and strong dust absorption limits. As predicted by the analytic model, to the right of this line, the ISRF becomes independent of X and depends only on τ_* (increasing with decreasing τ_*), whereas to the left of τ_{*crit} the ISRF intensity depends only on X . As shown by the top and right axis, τ_* is proportional to the DGR, and X is proportional to the galactic scale radius. The additional (weak) dependence of τ_* and X on the SFR reflects the fact that as the SFR increases, the typical distance to nearby source decreases (see §2.2). This in turn results in a weak increase of I_{UV}/Σ'_{sfr} with increasing SFR density.

Eq. (23) (and Fig. 4) cannot be directly compared to the FUV ISRF in the solar neighbourhood because of the assumption of a central observer. In contrast, in the Milky-Way, the solar galactocentric radius, $R_{\odot} = 8.5$ kpc, is large compared to the OB galactic scale radius, $R_{gal} = 3.5$ kpc. We shall now generalize Eq. (23) to the case of a non-central observer.

3.4. Non-central Observer

When the observer is located off the disk center the polar symmetry is broken and the problem becomes more complicated. In analogy to Eq. (18), we may write the ISRF as

$$\frac{F}{\Sigma_*} = \frac{e^{-\tau_* \bar{x}_0}}{4\pi \bar{x}_0^2} + \int_0^{2\pi} \int_{\bar{x}_0}^{\infty} \frac{1}{4\pi x} e^{-\tau_* x - g(\frac{x}{X}, \delta, \theta)} dx d\theta. \quad (24)$$

Here we defined

$$g \equiv \left[\left(\frac{x}{X} \right)^2 + 2\delta \left(\frac{x}{X} \right) \cos \theta + \delta^2 \right]^{1/2} - \delta. \quad (25)$$

Recall $\delta = R_{obs}/R_{gal}$ is the galactocentric radius of the observer relative to the galactic scale radius. In the limit $\delta \ll 1$, the function $g \rightarrow x/X$ and Eq. (24) approaches Eq. (18). When δ is not small, the integral cannot be solved analytically. However, as F/Σ_* is normalized to the local density of sources, its variation with the observer position is mild. This is because a significant fraction of the ISRF is always contributed by sources close to the observer. In fact, when τ_* is large such that $\tau_{gal} \gg 1$, F/Σ_* becomes independent of the observer position (and of X), as the ISRF is coming exclusively from sources close to the observer (whose density is characterized by Σ_*). Galactic gradients are then insignificant. On the other hand, when τ_* is small, sources at distances of order R_{gal} are contributing to the ISRF and F/Σ_* then depends on δ (and on X).

Motivated by this analysis, we seek a simple approximation for F/Σ_* (or, equivalently I_{UV}/Σ'_{sfr}) that obeys the above criteria. By examining our numerical results, we find that Eqs. (18) and (23) may be used to describe off-center observers under the replacement

$$\begin{aligned} \bar{x}_0 &\rightarrow \bar{x}_{\delta} \equiv \bar{x}_0 (1 - 0.1\delta^{0.5}) \\ X &\rightarrow X_{\delta} \equiv X (1 + 2\delta^2). \end{aligned} \quad (26)$$

where $\bar{x}_0 = 0.9$ (Eq. 22). This form has the desired behaviour discussed above: 1) For a central observer, $\bar{x}_{\delta} = \bar{x}_0$ and $X_{\delta} = X$, and Eqs. (18, 23) are unaltered. 2) In the strong-dust-absorption regime, at $Z'_d > Z'_{d,crit}$, the ISRF remains insensitive to δ . This is because in Eq. (26), the strongest dependence on δ is in X_{δ} . However, in this regime the ISRF is in any case only a function of τ_* . 3) In the weak-dust-absorption limit, the ISRF does vary with δ , as non local sources are important contributors to the flux. The fact that the ISRF *increases* with δ , reflects the increased contribution of sources towards disk-center, where Σ_* is exponentially higher.

A direct comparison of the numerical and analytic results for the entire parameter space is presented in Fig. 5. Note that in this plot the span of τ_* and X vary with δ (the hatched regions are regions not covered by our simulations) because our numerical galaxy models are defined by the central galaxy quantities (τ_{*c} , X_c) (see §2.3). In contrast τ_* and X are the local quantities (at the observer position), and they vary with δ (see Eq. 15). For most of the parameter space considered the analytic approximation and numerical results are in good agreement, on the level of $\lesssim 10\%$ relative difference.

In Fig. 6 we show I_{UV}/Σ'_{sfr} as a function of the τ_* and X (at the observer position), as given by our analytic solution, Eq. (22, 23, 26) (upper panels), and as obtained by our numerical simulations (bottom panels), for observers located at $\delta = 1$, and 2.4. In the right panels we mark the point that corresponds to the solar circle, for which $\delta = 2.4$, $\tau_* = 0.37$ and $X = 29$ (see §2.2). At this point $I_{UV}/\Sigma'_{sfr} = 1$, by definition. Comparing the results for $\delta = 1$ and 2.4, as well as with the central observer case $\delta = 0$ (Fig. 4) we see that for high τ_* and/or high X , the ratio I_{UV}/Σ'_{sfr} remains weakly sensitive to δ . As discussed above, this is because in the strong dust absorption limit the ISRF is generated by nearby sources, and thus when normalized to the local emissivity $\Sigma_* \propto \Sigma'_{sfr}$, it becomes insensitive to the observer position. However, when

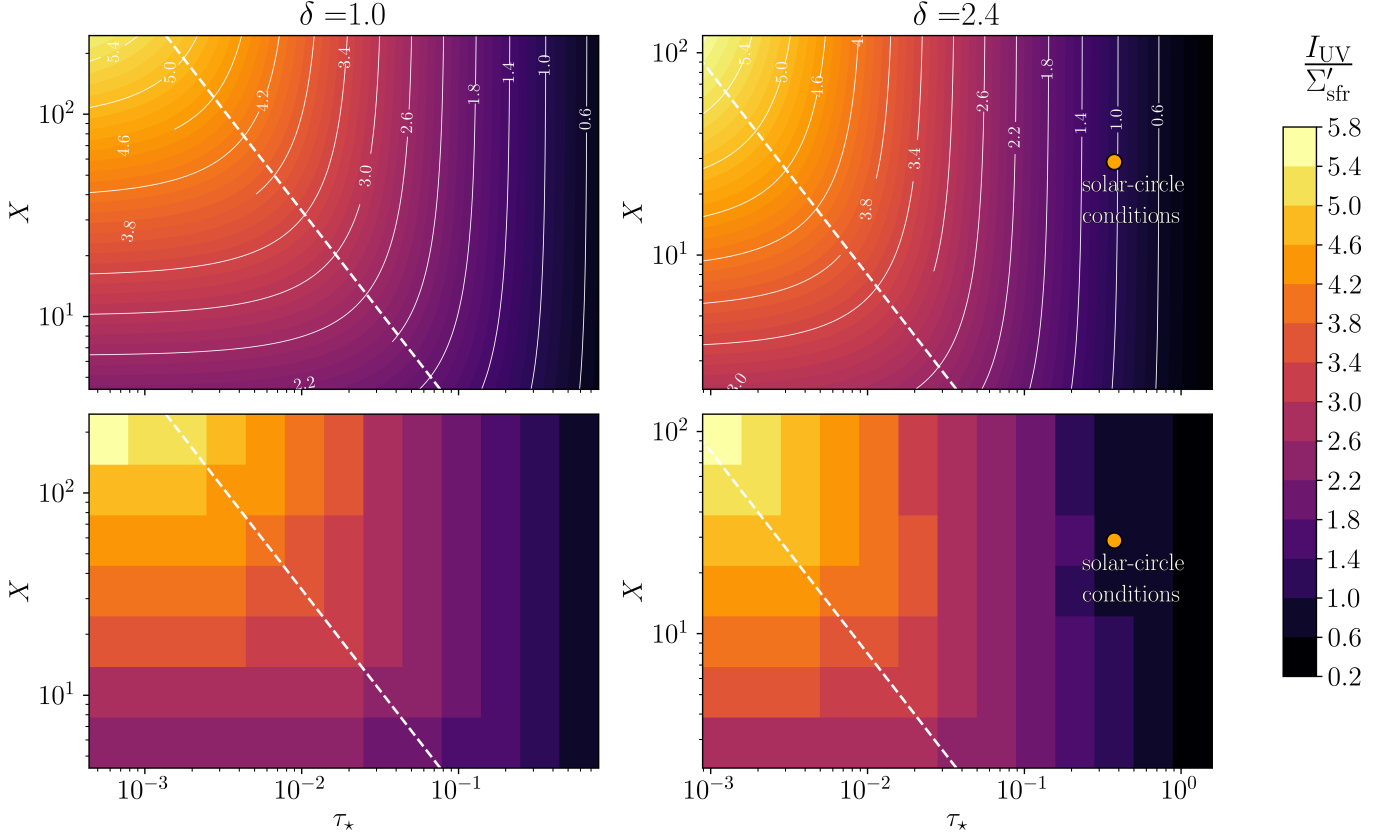


FIG. 6.— As Fig. 4 but for non-central observers, $\delta = R_{\text{obs}}/R_{\text{gal}} = 1$ and 2.4. The dashed line is the modified $\tau_{*,\text{crit}}$ (Eq. 27). The solar circle conditions are indicated.

τ_* is small and/or when X is small, sources at distances on the order of the galactic scale contribute significantly to the ISRF buildup, and $I_{\text{UV}}/\Sigma'_{\text{sfr}}$ is δ -dependent. For peripheral observers (e.g., at $\delta = 2.4$), $I_{\text{UV}}/\Sigma'_{\text{sfr}}$ increases above the values seen by a central observer. For example, for $X = 50$ and at the smallest τ_* , we see that $I_{\text{UV}}/\Sigma'_{\text{sfr}}$ increases from ≈ 3.8 at $\delta = 0$ (Fig. 4; bottom panel), to 4.4–5.2 at $\delta = 1 - 2.4$ (Fig. 6; bottom panels). This increase results from the contribution of faraway sources towards the galaxy center where the density of sources is high compared to that at the observer position.

A varying observer position also alters the location of the transition line from strong-to-weak dust absorption regimes. For a central observer we had $\tau_{*,\text{crit}} = 1/X$. Similarly, for a non-center observer we have

$$\tau_{*,\text{crit}} = 1/X_{\delta} = (1 + 2\delta^2)^{-1} X^{-1}, \quad (27)$$

or in terms of the DGR

$$Z'_{d,\text{crit}} = 0.32(n_0 R_{\text{gal,kpc}})^{-1} (1 + 2\delta^2)^{-1}. \quad (28)$$

Thus, $\tau_{*,\text{crit}}$ and $Z'_{d,\text{crit}}$ decrease with δ , and a larger region in the parameter space is occupied by the strong-dust absorption regime. The critical $\tau_{*,\text{crit}}$ as given by Eq. (27) is shown by the diagonal dashed lines in Fig. 6. Eq. (27) is in qualitative agreement with the numerical results where we see that with increasing δ the transition from the strong-to-weak dust absorption regime shifts down and to the left towards lower τ_* and X values. However, a quantitative comparison shows that Eqs. (27–28) under-estimate $\tau_{*,\text{crit}}$ and $Z'_{d,\text{crit}}$ at large δ .

4. SUMMARY AND DISCUSSION

4.1. Summary

In this paper we have studied how the FUV ISRF strength varies with galactic properties, the dust to gas ratio, the galaxy scale radius, the gas density, and the star-formation rate density. Two basic dimensionless parameters encapsulate these dependencies:

1. the opacity over the inter-source distance, $\tau_* = \sigma n l_*$
2. and the dimensionless disk radius $X = R_{\text{gal}}/l_*$

(Eq. 13). The ISRF intensity to the SFR density ratio is described by

$$\frac{I_{\text{UV}}}{\Sigma'_{\text{sfr}}} = 0.91 \left(\frac{e^{-\tau_* \bar{x}_0}}{2\pi \bar{x}_0^2} + E_1 \left[\bar{x}_0 \tau_* + \frac{\bar{x}_0}{X} \right] \right)$$

(Eq. 23), where the parameter $\bar{x}_0 = 0.9$ accounts for varying luminosity FUV sources, i.e., OB stellar associations. Eq. (23) also applies for off-center locations in the galaxy disk under the replacement $\bar{x}_0 \rightarrow 0.9(1 - 0.1\delta)$ and $X \rightarrow X(1 + 2\delta^2)$ (Eq. 26) where $\delta = R_{\text{obs}}/R_{\text{gal}}$ is the ratio of the galactocentric radius of the observer to the galactic scale radius of the OB stars. Over most of the parameter space considered, Eq. (23, 26) is accurate to the level of 10%.

There are two basic regimes in the problem, the strong and weak dust-absorption regimes, separated by the critical line $\tau_{*,\text{crit}} = 1/X$ or the critical dust-to-gas ratio $Z'_{d,\text{crit}}$ (Eq. 20, 21, or Eqs. 27, 28 for $\delta > 0$). In the weak-dust absorption regime ($Z' < Z'_{d,\text{crit}}$), the limit applicable to low metallicity dwarf and high redshift galaxies, sources on galactic scales contribute to the ISRF and $I_{\text{UV}}/\Sigma'_{\text{sfr}}$ is determined solely by

the X parameter. In this limit the ISRF intensity increases with the galactic scale radius. On the other hand, in the strong-dust absorption limit ($Z' > Z_{d,crit}$), i.e., the limit applicable to the Milky-Way, the ISRF is limited by dust absorption. In this limit I_{UV}/Σ'_{sfr} is determined solely by the τ_* parameter, and I_{UV}/Σ'_{sfr} then increases with decreasing τ_* (or with decreasing DGR or gas density).

4.2. Regulation of Star-Formation

Star formation in galactic disks may be self regulated by a natural feedback process that occurs in the multiphase ISM. Theories and observations suggest that the neutral ISM is dominated by two phases, the diffuse-warm ($T \sim 10^4$ K) and dense-cold (~ 100 K) neutral media (WNM and CNM), where the CNM-WNM are in rough pressure equilibrium with a density contrast of ≈ 100 (e.g., Field et al. 1969; Heiles & Troland 2003; Wolfire et al. 2003; Murray et al. 2018; Bialy & Sternberg 2019). These phases are steady-states at which the cooling and heating rates are equal. The feedback loop operates as follows: If the SFR of a galaxy (or a region in a galaxy) increases significantly, the intensity of the FUV ISRF also increases and results in excessive gas heating (through the photoelectric heating process) which results in the removal of the cold phase. Since star-formation is efficient in cold and dense gas, this in turn leads to a reduction in the star-formation rate. This feedback loop has been at the base of the star-formation regulation theory of Parravano (1988, 1989) and Ostriker et al. (2010).

A key ingredient in the star-formation self-regulation theory is how much gain in the FUV ISRF is produced per SFR density, i.e., what is the I_{UV} -to- Σ'_{sfr} ratio, where the I_{UV} parameter determines the thermal pressure of the multiphase neutral ISM (Wolfire et al. 1995; Bialy & Sternberg 2019). Following Ostriker et al. (2010), this thermal pressure (with additional pressure from turbulent motions) must balance the galactic disk weight which is determined by the stellar and dark matter density and gas surface density of the disk. Ostriker et al. (2010) assumed a constant ratio for I_{UV}/Σ'_{sfr} independent of galactic properties (see their Eq. 16). Our finding that the I_{UV}/Σ'_{sfr} ratio increases towards low metallicities implies that for the galaxy to still maintain a thermal pressure that allows a multiphase ISM, the SFR density must be reduced. This means that low metallicity galaxies are naturally pushed to have a lower star-formation efficiency (SFR density divided by gas column density), compared to their high metallicity counterparts, i.e., a lower normalization for the Kennicutt-Schmidt relation (e.g., Schmidt 1959; Kennicutt, Jr. 1998; Bigiel et al. 2008).

More recent studies (Kim et al. 2011; Ostriker & Shetty 2011; Shetty & Ostriker 2012; Kim et al. 2013; Kim & Ostriker 2015, 2017) focused on the role of turbulent pressure, generated by SN momentum injection as the dominant SFR regulation mechanism. These studies find that for a given SFR density, the turbulent pressure surpasses the thermal pressure, and thus suggest that SN feedback controls the SFR. Our finding that the I_{UV} -to- Σ'_{sfr} ratio increases in low metallicity galaxies implies that thermal pressure may dominate over turbulent pressure potentially reviving the role of FUV heating of the multiphase ISM as the dominant regulator of star-formation in these galaxies. This opens up a window for a bimodality in the star-formation process in galaxies, where in high metallicity galaxies it is controlled by SN feedback, whereas in low metallicity galaxies it is controlled by FUV heating

of the multiphase ISM. We note that at sufficiently low dust abundances, yet another transition occurs, as photoelectric heating becomes inefficient and other heating mechanisms become dominant: X-ray, cosmic-ray, and H₂-formation heating (Bialy & Sternberg 2019).

4.3. The Advantage of Using Dimensionless Quantities

Identifying the dimensionless parameters and rewriting the problem (and solving it) in dimensionless form (i.e., F/Σ_* as a function of τ_* and X ; Eqs. 16, 18) has a big advantage. It makes the results more general and enables future modifications to any assumed values and/or scaling relations to physical parameters that enter the model. For example, if one wishes to revise the value of the dust absorption cross section (here assumed to be $\sigma_g = 10^{-21}$ cm²), all one needs to do is to re-scale the relation between τ_* and Z'_d accordingly (Eq. 13). The numerical and analytic results for f in terms of τ_* are still valid and unchanged, it is only the translation from τ_* to Z'_d that changes. Similarly, any variations to our assumed relation for the source emissivity and SFR (Eq. 11), do not affect our results for the dimensionless flux, f , as f only depend on the dimensionless quantities, τ_* and X . Such a variation will of course affect the flux in physical units, F/Σ'_{sfr} (or I_{UV}/Σ'_{sfr}). If one wishes to adopt a different normalization (or a different scaling relation) than the one we used, one has to simply re-scale the I_{UV}/Σ'_{sfr} that we computed, accordingly (see for example, §4.4.1 below).

4.4. Limitations and Future Model Extensions

To be able to derive analytic formula for the variation of the ISRF with galactic properties we are forced to make simplifying assumptions. Here we discuss these assumptions and their validity.

4.4.1. Variations to the Initial Mass Function

To relate the source emissivity, Σ_* , to the SFR surface density, Σ'_{sfr} , we have assumed that the two are proportional with a proportionality factor calibrated based on solar neighborhood conditions (Eq. 11). If the stellar initial mass function (IMF) varies between galaxies, or within a galaxy, it would imply a variation in the adopted proportionality factor, as the sources that contribute to the ISRF are only the massive stars (mainly OB stellar types) which represent the high mass end of the IMF. For example, for a top heavy IMF, the fraction of massive stars is high compared to standard IMF (e.g. Kroupa 2002). This will imply a higher Σ_*/Σ'_{sfr} than adopted here. Whether the IMF is constant or varies with galactic properties is still under debate, and thus we do not include IMF variations as a component in our model. For a given IMF model it is possible to re-scale our results by adopting a non constant $\Sigma_* - \Sigma'_{sfr}$ proportionality factor that accounts for any potential systematic trend of the IMF with galactic properties, e.g., with metallicity (see §4.3).

4.4.2. Finite Disk Scale Height

In our models we have assumed thin disk geometry. This is a valid approximation if the radius over which a substantial contribution to the ISRF is accumulated, is large compared to the galactic scale height. We define $r_{1/2}$ as the radius within which half of the ISRF is accumulated. Exploring our numerical results we find that for large τ_* , $r_{1/2} \approx 2l_*$ (e.g., see Fig. 2). For low τ_* the total ISRF is higher as the contribution of distant sources is more substantial. In this case we

find $r_{1/2} \approx 5l_*$. Plugging the expression for l_* (Eq. 13) and comparing $r_{1/2}$ to the scale height we obtain the requirement:

$$H_{\text{OB}} \ll H_{\text{OB,crit}} \equiv 420 \Sigma_{\text{sfr}}'^{-1/2} \phi' \text{ pc}, \quad (29)$$

where H_{OB} is the scale height of OB stars, and where we defined $\phi' = (r_{1/2}/l_*)/3.5$. The factor ϕ' is close to unity, it varies from ≈ 1.4 at low τ_* down to ≈ 0.6 at high τ_* . Note that since H_{OB} is scale height of *only* the OB (massive) stars, it is much smaller than the stellar disk height which includes all stellar populations.

For typical condition Eq. (29) is satisfied. For example, in the Milky Way [Wolfire et al. \(2003\)](#) finds $H_{\text{OB}} = 59$ pc in the solar circle and towards smaller galactocentric radii, and an increasing trend towards larger galactocentric radii. In contrast, Σ_{sfr}' varies from ≈ 3.6 to ≈ 0.066 for radii $R = 4$ kpc to 18 kpc, implying $H_{\text{OB,crit}} = 220 - 1600$ pc. For very active starbursts, or very puffy disks, requirement (29) may be violated and a treatment of the disk width is needed. Another situation that requires considering the finite thickness of the disk is for studies of fluctuations of the ISRF distribution, in particular the high end of the ISRF distribution. This is because, as discussed in [PHM](#) the high end of the ISRF distribution often results from situations where the distance between the observer and the nearby source is abnormally small. For these cases $r_{1/2}$ will be smaller than the median $r_{1/2}$ value

discussed above, and may be smaller than H_{OB} . We generalize the theory to the case of finite disk thickness and study fluctuations in the FUV ISRF in a forthcoming study.

5. CONCLUSIONS

We have modeled the FUV interstellar radiation field both numerically and analytically. The ratio of the FUV ISRF intensity to the SFR density depends on the DGR (or metallicity), gas density, galactic scale radius and the SFR density. These dependencies are encapsulated in two controlling dimensionless parameters, τ_* and X . The $\tau_* - X$ parameter space is separated into two basic regimes, the weak and the strong dust absorption regimes, separated by the critical line $\tau_{*\text{crit}} = 1/X$, where for $\tau_* > \tau_{*\text{crit}}$ the ISRF is limited by dust absorption, and for $\tau_* < \tau_{*\text{crit}}$ it is limited by the galaxy scale radius. With decreasing τ_* (or decreasing metallicity), the ISRF intensity per SFR density increases, and reaches values a factor of 3-6 higher compared to disks like the Milky-Way. This may have important implications on the thermal state of the neutral ISM and the star-formation efficiency in low metallicity galaxies (e.g., dwarfs and high redshift galaxies), and may introduce a natural feedback loop for star-formation.

SB thanks David Hollenbach and Chris McKee for insightful discussions and useful comments. SB acknowledges support from the Harvard-Smithsonian Institute for Theory and Computation (ITC).

REFERENCES

- Bakes, E. L. O. & Tielens, A. G. G. M. 1994, *ApJ*, 427, 822
 Bialy, S., Burkhart, B., & Sternberg, A. 2017, *ApJ*, 843, 92
 Bialy, S. & Sternberg, A. 2016, *ApJ*, 822, 83
 —. 2019, *ApJ*, 881, 160
 Bigiel, F., Leroy, A., Walter, F., Brinks, E., de Blok, W. J. G., Madore, B., & Thornley, M. D. 2008, *AJ*, 136, 2846
 Corbelli, E. & Salpeter, E. E. 1988, *ApJ*, 326, 551
 Diemer, B., Stevens, A. R. H., Lagos, C. d. P., Caletto, A. R., Tacchella, S., Hernquist, L., Marinacci, F., Nelson, D., Pillepich, A., Rodriguez-Gomez, V., Villaescusa-Navarro, F., & Vogelsberger, M. 2019, *MNRAS*, 487, 1529
 Draine, B. T. 1978, *ApJS*, 36, 595
 Draine, B. T. & Bertoldi, F. 1996, *ApJ*, 468, 269
 Field, G. B., Goldsmith, D. W., & Habing, H. J. 1969, *ApJ*, 155, L149
 Glassgold, A. E. & Langer, W. D. 1974, *ApJ*, 193, 73
 Glover, S. C. O. & Clark, P. C. 2012, *MNRAS*, 421, 9
 Gnedin, N. Y., Tassis, K., & Kravtsov, A. V. 2009, *ApJ*, 697, 55
 Heiles, C. & Troland, T. H. 2003, *ApJ*, 586, 1067
 Hill, A. S., Mac Low, M.-M., Gatto, A., & Ibáñez-Mejía, J. C. 2018, *ApJ*, 862, 55
 Hollenbach, D. J. & Tielens, A. G. G. M. 1999, *Rev. Mod. Phys.*, 71, 173
 Kennicutt, Jr., R. C. 1998, *ApJ*, 498, 541
 Kim, C.-G., Kim, W.-T., & Ostriker, E. C. 2011, *ApJ*, 743, 25
 Kim, C. G. & Ostriker, E. C. 2015, *ApJ*, 802, 99
 Kim, C.-G. & Ostriker, E. C. 2017, *ApJ*, 846, 133
 Kim, C. G., Ostriker, E. C., & Kim, W. T. 2013, *ApJ*, 776, 1
 Kroupa, P. 2002, *Sci. (New York, N.Y.)*, 295, 82
 Krumholz, M. R., McKee, C. F., & Tumlinson, J. 2008, *ApJ*, 689, 865
 Kuhlén, M., Krumholz, M. R., Madau, P., Smith, B. D., & Wise, J. 2012, *ApJ*, 749, 36
 Leroy, A. K., Walter, F., Brinks, E., Bigiel, F., de Blok, W. J. G., Madore, B., & Thornley, M. D. 2008, *AJ*, 136, 2782
 Liszt, H. 2002, *A&A*, 389, 393
 McKee, C. F. & Krumholz, M. R. 2010, *ApJ*, 709, 308
 McKee, C. F. & Williams, J. P. 1997, *ApJ*, 476, 144
 Murray, C. E., Stanimirović, S., Goss, W. M., Heiles, C., Dickey, J. M., Babler, B., & Kim, C.-G. 2018, *ApJS*, 238, 14
 Ostriker, E. C., McKee, C. F., & Leroy, A. K. 2010, *ApJ*, 721, 975
 Ostriker, E. C. & Shetty, R. 2011, *ApJ*, 731, 41
 Parravano, A. 1988, *A&A*, 205, 71
 —. 1989, *ApJ*, 347, 812
 Parravano, A., Hollenbach, D. J., & McKee, C. F. 2003, *ApJ*, 584, 797
 Schmidt, M. 1959, *ApJ*, 129, 243
 Shetty, R. & Ostriker, E. C. 2012, *ApJ*, 754, 2
 Sternberg, A., Petit, F. L., Roueff, E., & Bourlot, J. L. 2014, *ApJS*, 790, 10S
 Tielens, A. G. G. M. & Hollenbach, D. 1985, *ApJ*, 291, 722
 Wolfire, M., Hollenbach, D., McKee, C., Tielens, A., & Bakes, E. 1995, *ApJ*, 443, 152
 Wolfire, M. G., McKee, C. F., Hollenbach, D., & Tielens, A. G. G. M. 2003, *ApJ*, 587, 278